JACS
JOURNAL OF THE AMERICAN CHEMICAL SOCIETY
Article
pubs.acs.org/JACS

Vibrational Signatures of Electronic Properties in Oxidized Water: Unraveling the Anomalous Spectrum of the Water Dimer Cation

Justin J. Talbot,[†,‡] Xiaolu Cheng,[†,‡] Jonathan D. Herr,[†,‡] and Ryan P. Steele*[,†,‡]

[†]Department of Chemistry, University of Utah, 315 South 1400 East, Salt Lake City, Utah 84112, United States
[‡]Henry Eyring Center for Theoretical Chemistry, University of Utah, 315 South 1400 East, Salt Lake City, Utah 84112, United States

Supporting Information

ABSTRACT: The water dimer cation, $(H_2O)_2^+$, has long served as a prototypical reference system for water oxidation chemistry. In spite of this status, a definitive explanation for the anomalous—and dominant—features in the experimental vibrational spectrum [Gardenier, G. H.; Johnson, M. A.; McCoy, A. B. *J. Phys. Chem. A*, **2009**, *113*, 4772−4779] has not been determined, and harmonic analyses qualitatively fail to reproduce these features. In this computational study, accurate quantum chemistry methods are combined with a fully coupled, six-dimensional anharmonic model to show that the unassigned bands are the result of resonant mode interactions and strong anharmonic coupling. Such coupling is fundamentally due to the unique electronic structure of this open-shell ion and the manner in which auxiliary modes affect the natural charge-transfer properties of the shared-proton stretch. These unique vibrational signatures provide a key reference point for modern spectroscopic and mechanistic analyses of water-oxidation catalysts.

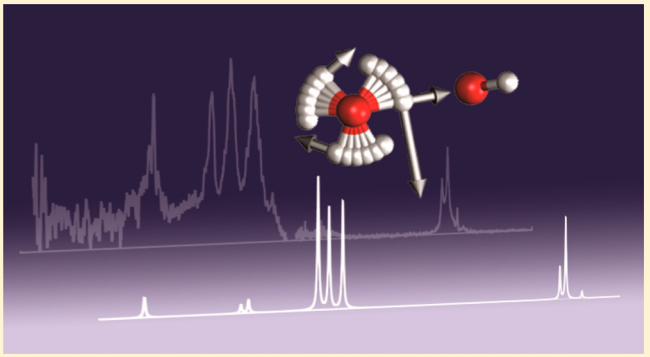

INTRODUCTION

The search for safe, clean, storable, and renewable energy sources remains one of the major scientific goals of our time. One potentially fruitful avenue for renewables is the storage of solar energy in chemical bonds,[1,2] such as the electrochemical splitting of water into molecular hydrogen and oxygen.[3−5] The water-splitting process provides as many questions for the field of chemistry, however, as it provides promises for renewable-energy technologies. Many viable catalysts have been developed for the more difficult water-oxidation process,[4,6−33] for example, but unraveling the detailed, inner-sphere redox mechanisms[34−40] remains a challenge that hampers continued progress toward the development of efficient, robust catalysts.[10]

The chemical activation of water involves substantial perturbations to chemical bonds and the surrounding hydrogen-bond network. Such inner-sphere changes, in turn, manifest as vibrational signatures. This concept is the premise for several recent gas-phase spectroscopic studies of water-oxidation catalysts,[41−48] which provide rare, experimental glimpses into these molecular mechanisms. A common refrain in many of these studies is that the observed spectra are appreciably more complicated than those predicted by harmonic analyses, even at very low temperatures. Anharmonicities can manifest as both strong shifts to the vibrational frequencies—well beyond traditional scaling factors—and the carrying of significant oscillator strength by higher-order effects, such as combination bands and overtones.

Such complexities could likely have been predicted, based on the precedent set by the anomalous—and as-yet unexplained—vibrational spectrum observed for the *simplest* model of the first redox step of water oxidation, the water dimer cation, $(H_2O)_2^+$ [Figure 1 inset].[49] The cold, argon-tagged action spectrum of this open-shell ion is dominated by intense transitions that are entirely absent in harmonic simulations, even with highly accurate quantum chemistry methods. Similar features are now known to occur in larger oxidized clusters, $(H_2O)_{n=3-11}^+$, as well.[50,51]

The objective of the present computational study, therefore, is to assign these anomalous features and connect such spectroscopic signatures to the inherent vibrational motions in oxidized water. The analysis demonstrates that the water dimer cation is an exquisite example of the coupling between electronic properties and molecular motion, as well as a rare case in which the immense broadening of strongly hydrogen-bonded spectral peaks (even in cold systems) can be ascribed to specific vibrational transitions. The vibrational signatures of electronic properties are exactly the observables sought in spectroscopic studies of water oxidation catalysts; this work highlights the underlying source of these signatures.

Oxidized water has been the subject of many previous computational studies, ranging from detailed electronic analyses of the dimer[52−58] to simulations of the condensed-phase

Received: July 15, 2016
Published: August 16, 2016

DOI: 10.1021/jacs.6b07182
J. Am. Chem. Soc. 2016, 138, 11936−11945

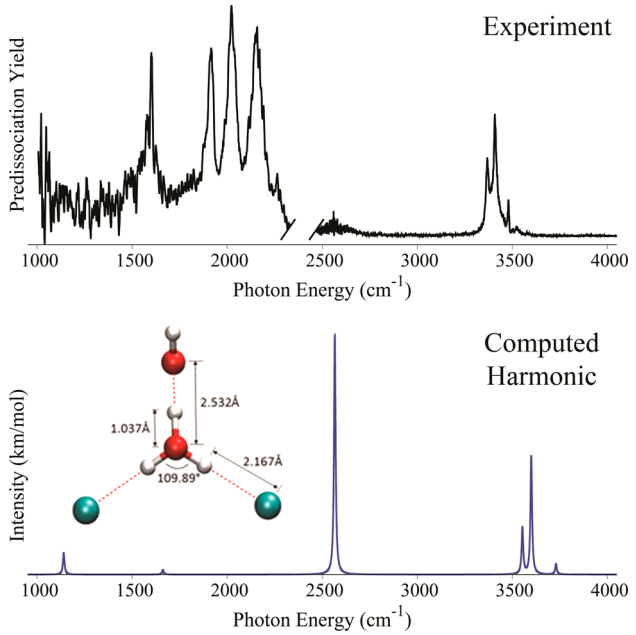

Figure 1. Comparison between the experimental[49] (top) and harmonic (bottom) spectra of the Ar-tagged water dimer cation $(H_2O)_2^+$ Ar_2. Calculations were performed with the RI-MP2/cc-pVTZ method. The inset shows the structure and geometric parameters at the reference structure, as discussed in the Methods section.

dynamics of bulk water ionization.[59,60] The structural studies have conclusively shown that (a) electron correlation effects are substantial in this open-shell ion, and (b) the proton-transferred (PT) isomer [Figure 1], nominally viewed as an ion-radical contact pair, $H_3O^+\cdots OH^\bullet$, is appreciably more stable than the hemibonded (HB) isomer. More recent experimental[50,51] and computational[61−63] studies, including two from our research group,[64,65] have established a clear driving force for an eventual separation of the initially formed ion-radical contact pair when sufficient solvation $[(H_2O)_{n\geq 5}^+]$ is present. The surrounding water network acts as a better solvent than the hydroxyl radical and outcompetes OH for solvation of the ion.

Experimental signatures of the ionization dynamics and reactive intermediates have remained elusive,[56,57,59] however, and one of the ancillary aims of this work is to establish the methodological considerations required to accurately connect experimental vibrational spectra with computational simulations. In order to highlight the rather stark discrepancies between standard harmonic computations and the experimental results, the two spectra are shown in Figure 1. Even with an underlying correlated, wave function-based methodology[66] and large basis set (RI-MP2/cc-pVTZ[67,68]), the harmonic spectrum is clearly insufficient to even qualitatively reproduce the dominant experimental signatures. The harmonic approach *does* reasonably reproduce the transitions in the high-frequency (3350−3550 cm^{-1}) O−H stretch region, apart from standard[69] anharmonic shifts of 5−10%, suggesting that the structure and electronic structure methodology are potentially sufficient. These transitions include the dangling-OH stretches of the hydronium and hydroxyl units, with the former being slightly red-shifted experimentally due to the presence of the weakly bound argon tags. In the lower-frequency region (1500−2500 cm^{-1}), however, at least four intense transitions dominate the experimental spectrum, and the harmonic analysis only includes the nearly dark bend transitions and bright shared-proton stretch. The triplet feature near 2000 cm^{-1}, with peak spacings of roughly 100 cm^{-1}, is absent. A two-dimensional anharmonic analysis that accompanied the experimental study of ref 49 placed the shared-proton stretch fundamental in the vicinity of the bright triplet, but neither the triplet feature nor the increased intensity of the bend(s) was recovered. In our preliminary studies, further refinement of the quality of the potential surface was found to make little difference in the resulting spectrum. In fact, the simpler second-order Møller−Plesset perturbation theory[66]-based surface (MP2) was found to yield frequencies that were closer to those from very accurate equation-of-motion coupled-cluster methods (EOM-IP-CCSD[70−73]) than those from the CCSD method. Therefore, the inconsistency must lie in the treatment of the molecular vibrations and the limitations of the harmonic approximation.

The remainder of this study aims to explain these anomalous features and is guided by the following questions:

(1) What is the source of the bright triplet feature near 2000 cm^{-1}?
(2) Why does the bend (or bends) near 1600 cm^{-1} carry considerable oscillator strength?
(3) What electronic properties of the water dimer cation manifest as these vibrational features?

METHODS

The design of this computational experiment was intended to reproduce the previously unexplained features in the vibrational spectrum of $(H_2O)_2^+$ and to explain the inherent electronic properties of this complex that lead to the anomalous intensity of these features. Accordingly, careful consideration of both the electronic and vibrational aspects of the complex was required.

Electronic Methods. As mentioned in the Introduction, all analyses in the present study focused on the PT isomer, and the two tagging Ar atoms were included, in order to provide the most direct connection with experimental results. After preliminary tests with CCSD[74,75] and EOM-IP-CCSD methods, the MP2 method (within the resolution-of-the-identity[76−81] [RI-MP2] and frozen-core approximations) was confirmed to provide sufficient accuracy. The cc-pVTZ basis set was also confirmed to be converged for spectroscopic analysis and was used throughout. (Smaller basis sets, such as aug-cc-pVDZ, were able to recover the qualitative effects of this work, but because of the sensitivity of resonant effects to reference peak positions, basis set-induced shifts can alter the resulting intensity pattern.) All quantum chemistry computations were performed with a development version of the Q-Chem[82] software package.

Reference Structure. The low-energy structure of $(H_2O)_2^+$, as well as its Ar-tagged analogue, possesses a "canted" hydroxyl unit, which does not bisect the terminal H−O−H angle of its hydronium partner. A two-dimensional anharmonic analysis (including a hydroxyl rotation and the O···O−H terminal wag) demonstrated that the zero-point energy of this hydroxyl rotation sits above the very shallow barrier to conversion toward a symmetrically equivalent structure. Figure 2 depicts a one-dimensional cut through this potential, as well as the ground vibrational state along this motion. Because of the singly peaked and symmetric distribution, the molecule can be considered to possess C_s point-group symmetry, on average. This symmetric transition-state structure then established the reference structure for subsequent anharmonic analysis and additionally provided useful symmetry arguments to justify the coupling (or lack thereof) between vibrational modes. A previous possible conjecture[49] for the mysterious triplet feature was a vibrational progression stemming from the low-frequency (87 cm^{-1} harmonic) wag of the hydroxyl unit. This explanation can now be discounted for two reasons. First, the anharmonic analysis places the wag frequency (141 cm^{-1}) above the harmonic value and progression spacing. Second, all subsequent anharmonic analyses of the high-frequency portions of the spectrum

DOI: 10.1021/jacs.6b07182
J. Am. Chem. Soc. 2016, 138, 11936−11945

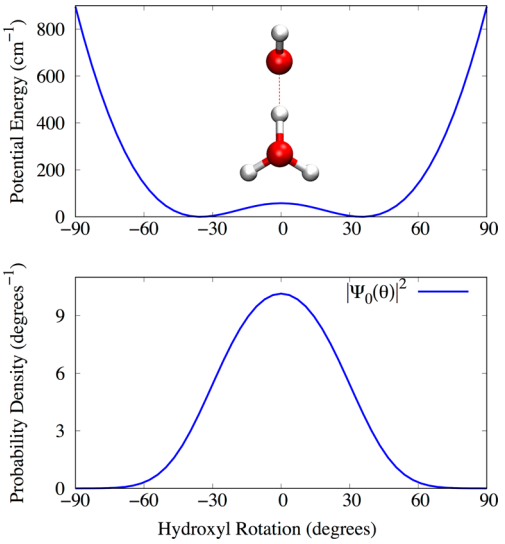

Figure 2. Potential energy surface along the hydroxyl rotation coordinate, with a fixed, equilibrium hydroxyl O−H bond length. The corresponding ground-state probability density, justifying the symmetric C_s transition-state reference structure, is shown in the lower panel.

showed little coupling to this wag motion. Therefore, the symmetric C_s structure was adopted as the reference point for all anharmonic analysis (Cartesian coordinates can be found in the Supporting Information), and the wag motion was neglected in the anharmonic simulations.

Vibrational Methods. The discrepancy between the experimental vibrational spectrum and harmonic analyses suggests that an accurate treatment of anharmonicity, including coupling among vibrational states, is required. General methods for computing anharmonic vibrational spectra include classical[83−85] and quantum[86−89] dynamics approaches, as well as eigenstate-based techniques within perturbative[90−93] or variational[94−106] analogues of electronic structure theory methods. Regardless of the approach, generation of the underlying potential energy and dipole moment hypersurfaces can be accomplished using Taylor series expansions or grid-based methods that directly scan along these surfaces. Due to the strong anharmonicities and mode couplings anticipated for the water dimer cation, the approach adopted in the present study was decidedly brute-force, which was possible—although still computationally demanding—for this relatively small complex. (After presenting the results of this analysis, a simpler model will later be discussed, which could potentially be applied to larger complexes.) Exact, grid-based, variational eigensolver methods in a well-chosen subspace of the vibrational degrees of freedom were performed. After an extensive preliminary search, six vibrational modes that could potentially carry oscillator strength in the 2000 cm^{-1} region—or strongly impact those that do—were selected and included in a six-dimensional vibrational Hamiltonian. The included five normal modes (q_i) and their labels are shown in Figure 3. Choice of the sixth degree of freedom (q_R) was largely guided by a previous study[107] of embedded-hydronium spectra, in which the rotational motion of the hydronium subunit was shown to lead to strong combination-band activity with the bending motion, due to nonlinear response of the dipole moment (electrical anharmonicity). In the present case, a rigid rotation of the hydronium, with a constant reduced moment of inertia (I), was used (also shown in Figure 3); kinetic coupling terms involving this mode were confirmed to be small and were subsequently neglected. The choice of this curvilinear coordinate was critical to reducing the number of coupled degrees of freedom and to interpretation of the spectrum. The resulting 6D Hamiltonian is, therefore,

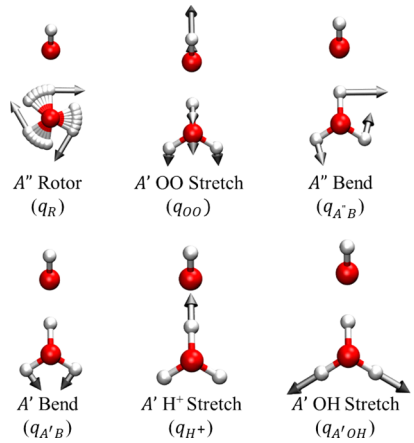

Figure 3. Vibrational modes included in the 6D anharmonic analysis. Argon atoms are omitted, for clarity.

$$\hat{H}_{\text{vib}} = -\frac{\hbar^2}{2I}\frac{\partial^2}{\partial q_R^{\,2}} - \sum_i^5 \frac{\hbar^2}{2m_i}\frac{\partial^2}{\partial q_i^{\,2}} + V(q_R, q_{OO}, q_{A''B}, q_{A'B}, q_{H^+}, q_{A'OH}) \quad (1)$$

Solution of the (J = 0) Schrödinger equation in this subspace was performed numerically in a basis set of harmonic oscillator functions. Six quanta of excitation were included in all modes except the shared-proton stretch, which required 10 quanta. Gauss-Hermite quadrature was used for integration of the potential energy and dipole moment terms; in each degree of freedom, the number of quadrature points was one larger than the number of states, requiring a total of over 184 000 quantum chemistry calculations. The large size of the resulting Hamiltonian matrix ($\sim 6 \times 10^9$ elements, before symmetry considerations) required the use of an iterative diagonalization routine, for which the PRIMME[108] library was employed. All of these anharmonic vibrational calculations were performed using in-house code, outside of Q-Chem.

Resonance Overview and Simplified Models. One important implication of mechanical anharmonicity is the phenomenon of resonance, which will play a key role in the interpretation of the unique features of this spectrum. Vibrational resonance provides an intensity-borrowing mechanism when two nearly degenerate vibrational states (of the same symmetry) have a non-negligible anharmonic coupling.[109] Qualitatively, strong coupling among two vibrational states can lead to strong mixing of the states; when this mixing occurs among a pair of bright and dark states, sharing of intensity can induce oscillator strength in nominally dark modes. Because this effect primarily affects two key transitions, a simplified, reduced-dimensional treatment of these resonant effects was conjectured to be possible. These reduced-dimensional models, along with exact, reduced-dimension eigensolvers, will be used throughout the discussion that follows, in order to confirm that the resonant interactions are responsible for the dominant spectral effects and also to assess the extent to which other modes impact the numerical accuracy of the final spectrum.

The resonance phenomena observed in this work are known as Fermi (overtone/fundamental [Type I] and combination band/fundamental [Type II]) and Darling−Dennison (fundamental/fundamental) resonances. Although the main numerical results in this work were constructed from fully nonlocal, grid-based scans of the potential and dipole surfaces, the dominant contributions to these two resonant effects can be ascribed to third- and fourth-order force constants,

$$\alpha^{(3)}_{ijk} = \frac{\partial^3 V}{\partial q_i \partial q_j \partial q_k}, \quad \alpha^{(4)}_{iiij} = \frac{\partial^4 V}{\partial q_i^{\,3} \partial q_j} \quad (2)$$

DOI: 10.1021/jacs.6b07182
J. Am. Chem. Soc. 2016, 138, 11936−11945

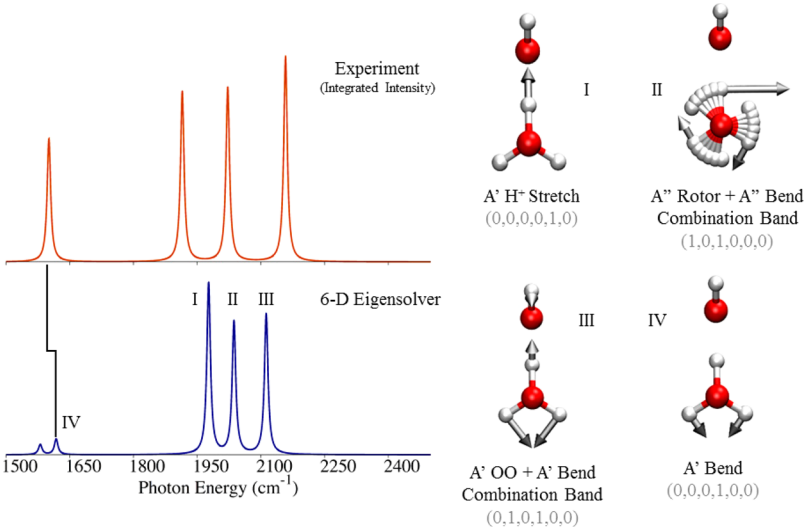

Figure 4. (Left) Comparison between the experimental and computed six-dimensional spectra. The intensity profile was computed by integrating the experimental peaks and normalizing the resulting spectra. (Right) Assignment of labeled absorption bands, notated in the order (ν_θ, ν_{OO}, $\nu_{A''B}$, $\nu_{A'B}$, ν_{H^+}, $\nu_{A'OH}$), and their corresponding molecular displacements.

An approximate vibrational Hamiltonian[110] can be developed in the state space containing only the active modes. A two-state interaction, for example, is expressed in the unperturbed eigenfunction basis $|\psi_1\rangle \otimes |\psi_2\rangle$ as

$$\hat{H} = \begin{pmatrix} E_1 & \beta_{1,2} \\ \beta_{1,2} & E_2 \end{pmatrix} \tag{3}$$

In this analysis, the unperturbed states could be considered fundamentals, combination bands ($i \neq j$), or overtones ($i = j$). The coupling element β can, in turn, be expressed as

$$\beta_{1,2} = \langle\psi_1|\hat{V}|\psi_2\rangle \quad \beta_{1,2}^{(3)} \approx \alpha_{ijk}^{(3)}\langle\psi_1|q_i q_j q_k|\psi_2\rangle$$
$$\beta_{1,2}^{(4)} \approx \frac{\alpha_{iiij}^{(4)}}{6}\langle\psi_1|q_i^3 q_j|\psi_2\rangle \tag{4}$$

where the leading-order coupling terms are shown for Fermi ($\beta^{(3)}$) and Darling–Dennison ($\beta^{(4)}$) resonances. The generalized eigenvalues of (3) become

$$\omega_{1,2} = \frac{E_1 + E_2}{2} \pm \sqrt{\left(\frac{\delta}{2}\right)^2 + \beta^2} \tag{5}$$

where the spacing between the unperturbed energies has been defined as $\delta = E_1 - E_2$. The corresponding eigenvectors are, in general, a nonuniform superposition of basis states. The mixing coefficient (ζ) and normalized eigenvectors become

$$\zeta_\pm = \left(\frac{1}{2} \pm \frac{\delta}{2\sqrt{\delta^2 + 4\beta^2}}\right)^{1/2}, \quad |\Psi\rangle_\pm = \zeta_+|\psi_1\rangle \pm \zeta_-|\psi_2\rangle \tag{6}$$

Intensity borrowing, therefore, occurs via mixing of the two reference states via ζ. This process conserves intensity, and, in a case in which one state is rigorously dark, the resulting intensity is simply proportional to the square of the mixing coefficient. These models can be extended to additional states, and such analyses are included in the Supporting Information.

RESULTS AND DISCUSSION

The computed six-dimensional spectrum is shown in Figure 4, along with the qualitative assignment of absorption bands and corresponding nuclear motions. For visual comparison only, the integrated intensities of the experimental spectrum (obtained with the Origin[111] software package) are also presented in this figure with the same 10 cm^{-1} Lorentzian artificial broadening as the computed spectra. Quantitative frequencies and intensities are listed in Table 1.

Table 1. Comparison of Harmonic, Computed (6D) Anharmonic, and Experimental Spectra

	harmonic		anharmonic		experiment
mode	ω^a	I^b	ω^a	I^b	ω^a
A'' Rotor	(525)[c]	(0.9)[c]	504	0.00	—
A' OO Stretch	342	47.5	378	63.7	—
A'' Bend	1662	48.3	1581	55.9	—
A' Bend	1685	0.9	1618	87.0	1601
A' H$^+$	2566	2537.4	1977	948.1	1916
A' OH Stretch	3553	491.0	3460	466.6	3408
Comb 1[d]	—	—	2037	733.6	2021
Comb 2[e]	—	—	2113	777.4	2155

[a]Transition frequency (cm^{-1}) [b]Intensity (km/mol) [c]Values from rectilinear "rotor" normal mode [d][A' OO Stretch + A' Bend] combination band (0,1,0,1,0,0). [e][A'' Rotor + A'' Bend] combination band (1,0,1,0,0,0).

Most encouragingly, the intense triplet feature is recovered in the anharmonic simulations, which stands in stark contrast to the single bright shared-proton stretch peak that was observed in the harmonic analysis. On the basis of the resulting eigenvector coefficients, the triplet is ascribed to a strong Fermi resonance among the A' shared-proton stretch fundamental (q_{H^+}) and two 1 + 1 combination bands. These combination bands include the [A' OO stretch + A' HOH hydronium bend] mode, hereafter denoted q_{comb_1}, and the [A'' hydronium rotor + A'' HOH hydronium bend] mode, denoted q_{comb_2}. In addition, a weaker two-fundamental Darling–Dennison resonance between the A' hydronium bend and A' proton stretch fundamentals was observed, which modifies the position and intensity of the bend. Detailed analysis of each of these modes, along with the source of the strong anharmonic couplings, is provided in the following subsections. The transitions are referenced according to the labeling in Figure 4.

DOI: 10.1021/jacs.6b07182
J. Am. Chem. Soc. 2016, 138, 11936–11945

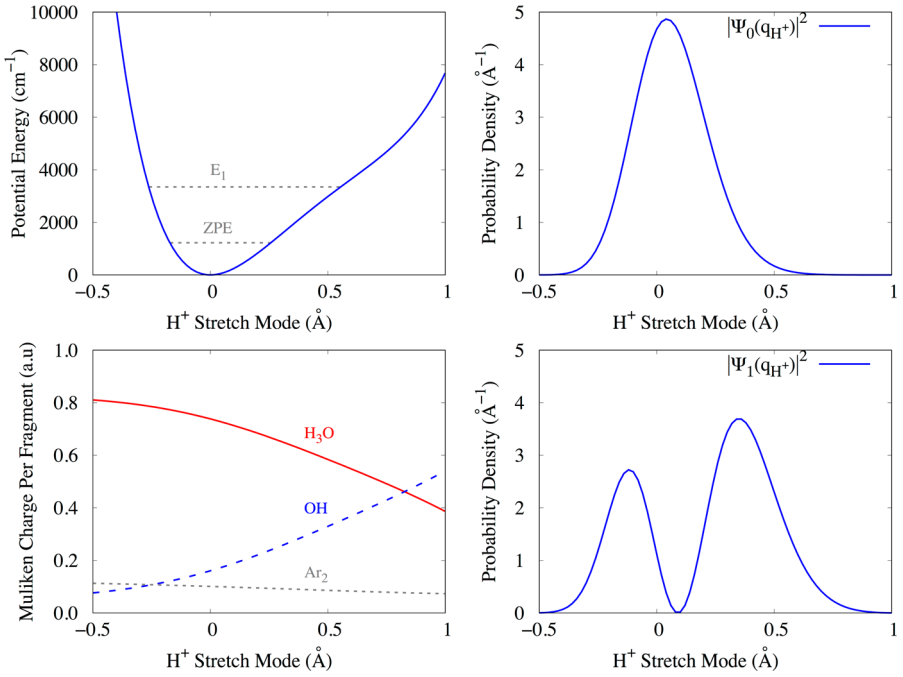

Figure 5. One-dimensional anharmonic analysis of the shared-proton stretch mode (q_{H^+}). (Upper left) Potential energy curve and two lowest energy eigenvalues, with corresponding eigenstate probability densities in the right two panels. (Lower left) Fragment partial charges as a function of q_{H^+} displacement.

Triplet Feature. *1. A′ Shared-Proton Stretch (Transition I).* Upon initial ionization,[56,59,60] the cationic water dimer undergoes rapid proton transfer to form the aforementioned ion-radical contact pair, in which the hydronium cation and hydroxyl radical are connected by a strongly anharmonic, proton-transfer coordinate. The anharmonicity and large intensity in this mode are critical pieces of the anomalous vibrational response and will receive special attention throughout this analysis. As a result of the strong anharmonicity, the shared proton undergoes large-amplitude motion, even in the ground vibrational state. At the minimum-energy structure, the shared-proton bond length is computed to be 1.037 Å (Figure 1). However, along the corresponding proton-stretch normal-mode coordinate (Figure 5), the 1D anharmonic expectation value of the bond length was computed to be $\langle\psi_0|q_{H^+}|\psi_0\rangle$ = 1.072 Å for the ground vibrational state and $\langle\psi_1|q_{H^+}|\psi_1\rangle$ = 1.152 Å for the first excited state.

Importantly, large-amplitude motion along this coordinate effectively shuttles the complex between $H_3O^+ \cdots OH^\bullet$ and $H_2O \cdots H_2O^{+\bullet}$ limiting regimes. The amount of charge transfer along the vibrational coordinate can be tracked using summed atomic charges on three fragments (Ar_2, H_3O^+, and OH) using simple Mulliken analysis,[112] shown in the lower-left panel of Figure 5. By 0.8 Å displacement along this coordinate, equal charges of the OH and H_3O subunits were observed; roughly 90% of this charge transfer has occurred at the classical turning points of the first excited vibrational state. This charge oscillation is responsible for the enormous intensity response of q_{H^+} in the harmonic spectrum and also acts as a potential "intensity donor" to other parasitic transitions in the anharmonic spectrum, as discussed below.

2. A″ Rotor + A″ Bend Combination Band (Transition II). The curvilinear rotor coordinate is one motion by which the charge-shuttling effect can be inhibited. At the hydrogen-bonded equilibrium, charge transfer is enabled, whereas charge localization is fostered upon a ± 60° rotation. This motion, when combined with the *A″* bend (to yield the *A′* combination band q_{comb_1}), has previously been shown to induce a bright combination-band transition in solvated hydronium complexes, by means of a non-Condon effect.[107] This effect induces oscillator strength through *electrical* anharmonicity even when the potential is nearly (or even purely) harmonic. Preliminary analysis of this effect in the water dimer cation, using only these two motions, showed that this combination-band activity was present, but the computed intensity remained appreciably lower than the experimentally observed response. Using the full 6D model, the correct response was instead found to be dominantly a *three*-mode effect in the present case, in which q_{comb_1} borrows intensity through a Fermi resonance with the bright shared-proton stretch. The rotor (504 cm^{-1}, anharmonically) and *A″* hydronium bend (1581 cm^{-1}) yield a combination band (2113 cm^{-1}) that fortuitously lands close to the original anharmonic shared-proton stretch fundamental (2126 cm^{-1}, 1D) and can borrow significant intensity from this otherwise-dominant peak. The two reference transitions then split, via a strong anharmonic, resonant coupling, to yield two of the three bright peaks in the triplet. Therefore, in the water dimer cation, the intensity of this additional peak originates from *both* mechanical and electrical anharmonicities.

Additional qualitative insight into this feature of the spectrum can be obtained by projecting the final, anharmonic state onto the direct-product, one-dimensional, harmonic basis. This projection, when properly accounting for relative phase, allows for visualization of the corresponding nuclear motion associated with the transition. In this case, q_{comb_1} primarily exhibits motion of the shared proton perpendicular to the proton-transfer coordinate, thereby hindering the proton-shuttling mechanism by partially breaking the hydrogen bond. The rotor motion partially cancels the terminal hydrogens' contribution to the

DOI: 10.1021/jacs.6b07182
J. Am. Chem. Soc. 2016, 138, 11936−11945

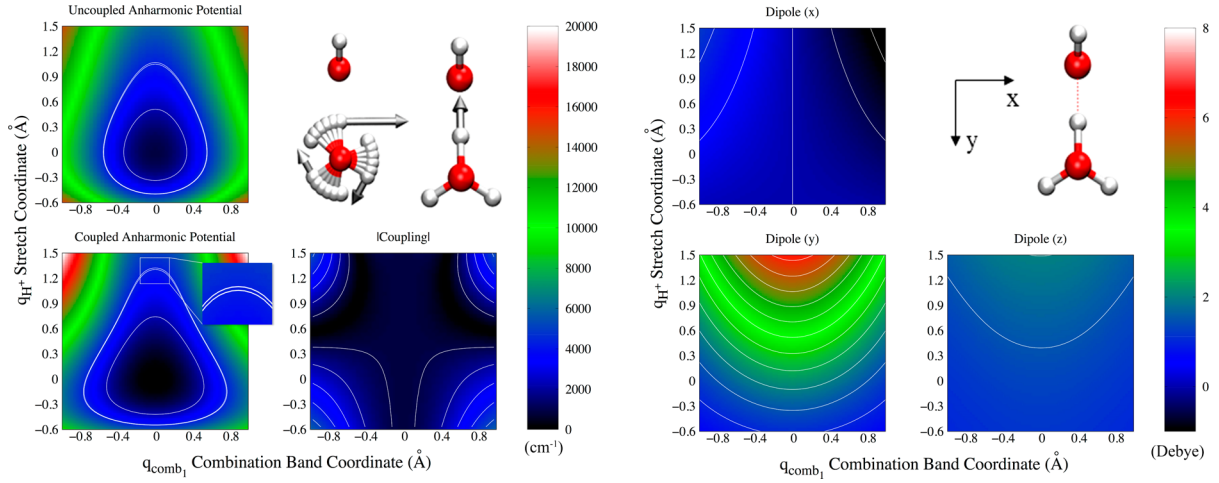

Figure 6. Potential energy and dipole moment surfaces for the shared-proton stretch coordinate (q_{H^+}), combined with the $[A''$ hydronium rotor + A'' bend$]_{1,1}$ combination band coordinate (q_{comb_1}). (Left panels) Uncoupled and coupled anharmonic potential energy surfaces, along with the coupling strength. The white contour lines in the potential plots denote the three lowest eigenvalues of the 6D eigensolver (the two resonant transitions are closely spaced). The contours in the coupling plot are placed every 1000 cm^{-1}. (Right panels) Dipole moment surfaces in the Cartesian directions, with the convention that the O−O axis is placed in the y direction of the x−y plane. Contour lines are placed every 0.5 D.

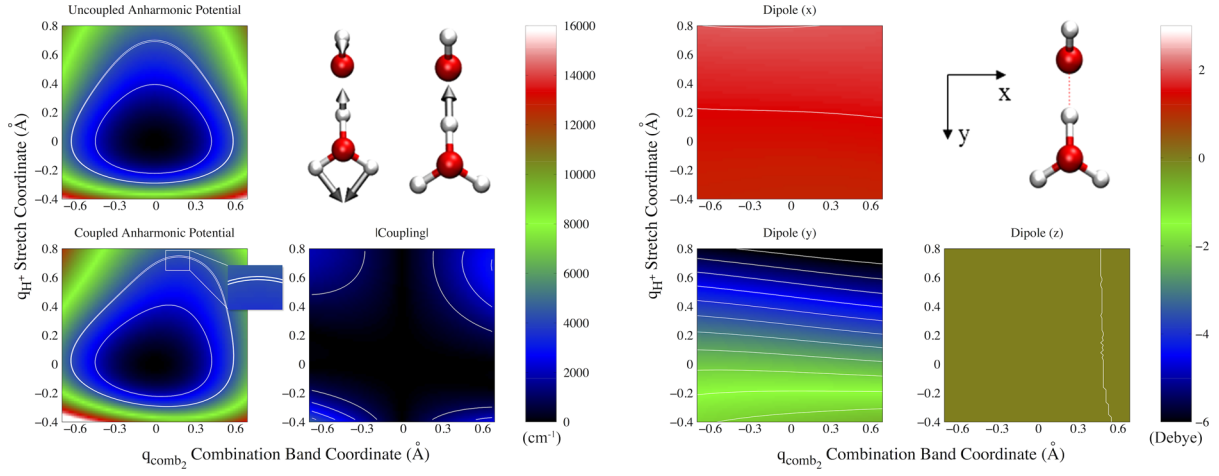

Figure 7. Potential energy and dipole moment surfaces for the shared-proton stretch coordinate (q_{H^+}), combined with the $[A'$ OO stretch + A' bend$]_{1,1}$ combination band coordinate (q_{comb_2}). (Left panels) Uncoupled and coupled anharmonic potential energy surfaces, along with the coupling strength. The white contour lines in the potential plots denote the three lowest eigenvalues of the 6D eigensolver (the two resonant transitions are closely spaced). The contours in the coupling plot are placed every 1000 cm^{-1}. (Right panels) Dipole moment surfaces in the Cartesian directions, with the convention that the O−O axis is placed in the y direction of the x−y plane. Contour lines are placed every 0.5 D.

bending motion, whereas it enhances the side-to-side motion of the central proton. From this decomposition, the combination-band coordinate can be dominantly considered as $q_{comb_1} = 0.87q_\theta + 0.44q_{A''B}$. The displacements corresponding to this motion are shown by arrows in Figure 6.

From an underlying electronic viewpoint, the charge-localizing behavior of this combination band motion strongly impacts the charge-delocalizing tendency of the proton stretch, which leads to a very large third-order coupling among these modes. This coupling is depicted visually in the potential energy surfaces of Figure 6. The two-state coupling matrix element between these two motions, for example, is $\beta^{(3)} = -56.0$ cm^{-1}, which closely matches a three-dimensional eigensolver splitting of ± 54.1 cm^{-1}, suggesting that a simplified two-state model should be reasonably consistent with exact eigensolvers, provided that the 2D combination-band coordinate is known in advance. Both the simplified 2D model and 3D eigensolver results are shown in Figure 8(a), which confirmed that these three modes are, in fact, responsible for two of the three contributions to the infrared activity in this region. The rotation coordinate also provides a strong electrical anharmonicity orthogonal to the shared-proton stretch coordinate (Figure 6), providing additional oscillator strength to the combination band.

Using the simplified, two-state Hamiltonian, with calculated matrix elements $E_1 = \langle 110|(E_{1,harm} + \Delta^{(2D)}_{1,anh})|110\rangle_{qcomb_1} = 2124.29$ cm^{-1} and $E_2 = \langle 001|(E_{2,harm} + \Delta^{(1D)}_{2,anh})|001\rangle_{H^+} = 2126.29$ cm^{-1}, the spectrum was modeled and decomposed to quantify the degree of state mixing. The parameters $\Delta^{(2D)}_{1,anh}$ and $\Delta^{(1D)}_{2,anh}$ were computed by scaling the harmonic combination-band and fundamental transition frequencies to their 2D and 1D anharmonic values, respectively. Because of the near degeneracy of the reference states, the mixing coefficients (6) provide a nearly equal mixing between the vibrational

DOI: 10.1021/jacs.6b07182
J. Am. Chem. Soc. 2016, 138, 11936−11945

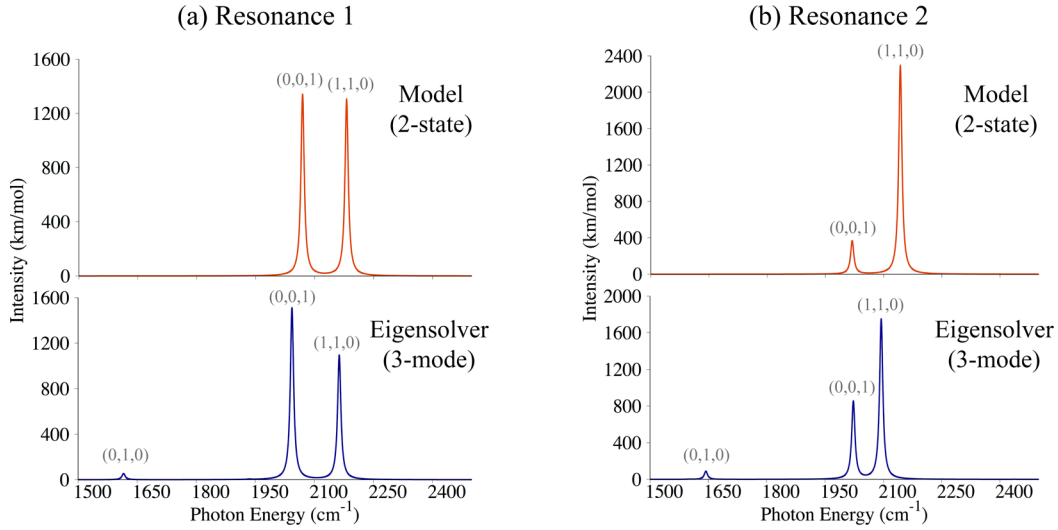

Figure 8. IR spectra resulting from the simplified 2D model and 3D eigensolver, involving the shared proton stretch (q_{H^+}), coupled to (a) q_{comb_1} and (b) q_{comb_2}. In (a), transition labels are denoted as (ν_{θ}, $\nu_{A''B}$, ν_{H^+}); in (b), transition labels are denoted as (ν_{OO}, $\nu_{A'B}$, ν_{H^+}).

eigenstates. The resulting spectrum is shown in Figure 8(a), and quantitative results of this model are listed in Table S2 of the Supporting Information.

3. A′ O−O Stretch + A′ Bend Combination Band (Transition III). The next Fermi resonance occurs between q_{comb_2} and the A' proton stretch fundamental. The uncoupled states are farther from resonance (≈450 cm^{-1}), compared to the previous case. In order for Fermi mixing to occur in the present pair, the required properties include a significantly stronger anharmonic coupling of these two states and/or appreciable perturbation to the states by other modes. The value of the mixed third derivative was, indeed, found to be large which provides the necessary term for appreciable mixing of the two states. This coupling is evident in the deviation between the uncoupled and coupled potentials depicted in Figure 7.

Although the strength of the two-state coupling matrix element ($\beta^{(3)}$ = 42.8 cm^{-1}) is comparable to the corresponding three-dimensional eigensolver splitting (±35.8 cm^{-1}), the mixing is actually lower than in the previous resonance, due to the slight off-resonant character of the reference states. As a result, the reduced-dimensional model somewhat overestimated the transition frequencies and the corresponding intensity profile [Figure 8(b)]. This effect is also impacted by some degree of coupling to the A' bend, which red-shifts the shared-proton stretch and allows for increased resonance in the 3D and 6D eigensolver treatments.

The expansion coefficients accordingly reveal that this combination band is dominated by the A' bend motion and can be adequately represented as q_{comb_2} = −0.25 q_{OO} + 0.97 $q_{A'B}$. The q_{OO} component also exhibits hydroxyl bend and out-of-plane (symmetry-conserving) shared-proton components, as shown by the arrows in Figure 7. The strong coupling of the resonant modes then has a rather intuitive electronic interpretation, using $H_2O\cdots H^+\cdots OH^\bullet$ reference fragments. Displacement along the symmetric bend (or along q_{comb_2}) appreciably alters the water lone pair to which the proton is bound, thereby changing its proton affinity and the stretch potential of the proton. Since the proton motion carries the "original" oscillator strength in the harmonic reference, strong modification of the proton stretch potential also alters the charge-transfer property and leads to both strong mechanical coupling and intensity borrowing. A smaller but nontrivial contribution also comes from the modification of the donor−acceptor distance—and, in turn, the proton-stretch potential—during the O−O stretch motion.

Bend Intensity. The experimental spectrum exhibits a bright signature in the bending region, as well. Of the A' and A'' bending motions, the A'' bend is the mode that carries appreciable oscillator strength, which is still much too low harmonically. However, a Darling−Dennison resonance was observed when the A′ mode was allowed to couple with the proton stretch fundamental. As a fourth-order effect that is reasonably off-resonance, the anharmonicity constant must be strong in order to induce intensity borrowing. Indeed, the quartic derivative term was found to be very large, yielding a coupling matrix element of β = −34.9 cm^{-1}. Qualitatively, this strong coupling occurs for reasons similar to the coupling of q_{comb_2} and the proton stretch: Motion along this bend, which moves the proton side-to-side, drastically modifies the stretch potential.

The off-resonant character of these two modes leads to little state mixing in the resultant eigenfunctions, which also does *not* yield the full intensity shown in the experimental spectrum. It does, however, lead to a 97-fold increase in the bend intensity, compared to the harmonic result, which, in this case, is due to mechanical coupling. Therefore, the mere appearance of the bend transition should be considered a success for this model. The remnant discrepancy with the experimental intensity remains unclear. While we are always hesitant to ascribe such inconsistency to experimental effects, neither improvements to the potential nor to the vibrational model led to appreciably increased intensity. Based on discussions with experimentalists regarding the reliability of the intensities in this region, the rather significant noise (including a poorly defined baseline) suggests that the bright intensity of the bend could, indeed, be viewed with some skepticism, particularly due to laser power in this region. If such signatures become key factors in studies of future catalysts, revisiting this region of the spectrum may be worthwhile.

DOI: 10.1021/jacs.6b07182
J. Am. Chem. Soc. 2016, 138, 11936−11945

High-Frequency A' O−H Stretch. Since the intensity of a resonant transition is directly proportional to the square of the mixing coefficient ($\zeta_{\pm}$), small shifts in any of the unperturbed frequencies can result in a large intensity change after mixing. This factor was one of the primary difficulties encountered during the computational analysis of this spectrum since such shifts can be induced by both the choice of electronic structure method[113−115] and by the choice of modes included in the model. On the latter front, inclusion of the exterior O−H symmetric stretch mode in the 6D model led to non-negligible shifts, and this last mode's effect on the spectrum provided sufficiently quantitative agreement with experiment. In all cases, the inclusion of this stretch led to changes in the value of δ (unperturbed energy gaps), with the largest shifts affecting the A' bend and the two aforementioned combination bands. By including the external O−H stretch, extension/contraction of the O−H bonds during the rotor and bend motions is allowed and provided an improved representation of these motions. Further analysis of this mode's influence on the spectrum, including higher-dimensional simplified model results, can be found in Figure S3 of the Supporting Information.

CONCLUSIONS

The vibrational spectrum of the water dimer cation—a prototypical model of ionized water—is dominated by intense transitions that are absent in harmonic analyses. Using an anharmonic eigensolver approach with accurate electronic structure theory, the analysis in this work has definitively assigned these transitions to resonant interactions between vibrational modes. In short, the proton stretch transition is sufficiently bright that nearly any other vibrational transition with proper frequency—including combination bands—can steal intensity and appear as an unexpectedly bright transition. Traditional anharmonic effects (shifting of the 1D frequencies) certainly impacted the final spectrum and were required for quantitative agreement, but the bulk of the effect was found to be multidimensional, involving resonant interactions and strong coupling between higher-order modes.

Broadening of proton-stretch peaks has been observed in cold spectra of many other systems.[116−122] The present complex is unique in that the source of these broadenings can be assigned to specific combination bands. Furthermore, the electronic origin of the strong coupling was assigned to particularly intuitive effects. The native shared-proton molecular motion, which facilitates electronic shuttling between $H_3O^+\cdots OH^\bullet$ and $H_2O\cdots H_2O^{+\bullet}$ reference structures, was found to be strongly enhanced/inhibited by motions that make/break hydrogen bonds. In fact, a nonquantitative, yet intuitive, interpretation of the dominant triplet feature is that it represents the motion along (y) and orthogonal to (x,z) the shared-proton stretch. The clear failure of the harmonic approximation suggests that the normal-mode reference picture is flawed for this system, and this proton-motion interpretation (with more quantitative inclusion of other motions, as described above) appears to suffice.

This study has been motivated by the need to understand the experimental vibrational signatures of practical water-oxidation catalysts, and it provides key comparison data for these signatures. Of course, water oxidation is a four-electron, four-proton redox process, and this analysis only focuses on the first of these four steps. Several lessons have been gleaned, however. First and foremost, the electronic properties of the inherent vibrational motion in water oxidation complexes can be inferred from a proper combination of modern experimental and computational infrared spectra. This facet is particularly encouraging for the rational design of improved catalytic complexes. Second, an improved computational framework is required if these effects are to be routinely assigned. In many spectra, these effects are benign features that barely rise above the baseline noise, making the harmonic approximation sufficient; however, due to the unique electronic structure of ion/radical systems, strong anharmonic coupling can promote such effects as the most intense features in the spectrum. Finally, the rich information contained in the intensities of these transitions suggests that continued focus should be placed—both experimentally and theoretically—on this region of the infrared spectrum, especially for water-oxidation catalysis studies. Often a region devoid of transitions between the high-frequency stretches and the fingerprint region, this strongly hydrogen-bonded region provides key information regarding the vibrational—and electronic—structure of reactive water species. Future focus will be placed on the infrared activity of larger model water complexes and recently developed catalysts.

ASSOCIATED CONTENT

Supporting Information

The Supporting Information is available free of charge on the ACS Publications website at DOI: 10.1021/jacs.6b07182.

Results for higher-dimensional, simplified models, as well as 4- and 5-D eigensolvers; Cartesian coordinates of reference structure for anharmonic computations (PDF)

AUTHOR INFORMATION

Corresponding Author

*ryan.steele@utah.edu

Notes

The authors declare no competing financial interest.

ACKNOWLEDGMENTS

The authors gratefully acknowledge Mark Johnson and Conrad Wolke for providing the original experimental spectroscopic data. Anne McCoy, Michael Morse, Mike Duncan, Gary Douberly, and Stephen LeBohec are also thanked for helpful discussions. This material is based upon work supported by the National Science Foundation CAREER under CHE-1452596. The support and resources from the Center for High-Performance Computing at the University of Utah are gratefully acknowledged. This work also used the Extreme Science and Engineering Discovery Environment (XSEDE), which is supported by National Science Foundation grant number ACI-1053575.

REFERENCES

(1) Lewis, N. S.; Nocera, D. G. *Proc. Natl. Acad. Sci. U. S. A.* **2006**, *103* (43), 15729−15735.
(2) Harriman, A. *Philos. Trans. R. Soc., A* **2013**, *371* (1996), 20110415.
(3) Kalisman, P.; Nakibli, Y.; Amirav, L. *Nano Lett.* **2016**, *16* (3), 1776−1781.
(4) Blakemore, J. D.; Crabtree, R. H.; Brudvig, G. W. *Chem. Rev.* **2015**, *115* (23), 12974−13005.
(5) Meyer, T. J. *Nature* **2008**, *451* (7180), 778−779.
(6) Kanan, M. W.; Nocera, D. G. *Science* **2008**, *321* (5892), 1072−1075.

DOI: 10.1021/jacs.6b07182
J. Am. Chem. Soc. 2016, 138, 11936−11945

(7) Hull, J. F.; Balcells, D.; Blakemore, J. D.; Incarvito, C. D.; Eisenstein, O.; Brudvig, G. W.; Crabtree, R. H. *J. Am. Chem. Soc.* **2009**, *131* (25), 8730−8731.
(8) Lutterman, D. A.; Surendranath, Y.; Nocera, D. G. *J. Am. Chem. Soc.* **2009**, *131* (11), 3838−3839.
(9) Surendranath, Y.; Dincă, M.; Nocera, D. G. *J. Am. Chem. Soc.* **2009**, *131* (7), 2615−2620.
(10) Bard, A. J. *J. Am. Chem. Soc.* **2010**, *132* (22), 7559−7567.
(11) Chen, Z.; Concepcion, J. J.; Luo, H.; Hull, J. F.; Paul, A.; Meyer, T. J. *J. Am. Chem. Soc.* **2010**, *132* (50), 17670−17673.
(12) Concepcion, J. J.; Jurss, J. W.; Norris, M. R.; Chen, Z.; Templeton, J. L.; Meyer, T. J. *Inorg. Chem.* **2010**, *49* (4), 1277−1279.
(13) Jurss, J. W.; Concepcion, J. C.; Norris, M. R.; Templeton, J. L.; Meyer, T. J. *Inorg. Chem.* **2010**, *49* (9), 3980−3982.
(14) Karunadasa, H. I.; Chang, C. J.; Long, J. R. *Nature* **2010**, *464* (7293), 1329−1333.
(15) Young, E. R.; Nocera, D. G.; Bulovic, V. *Energy Environ. Sci.* **2010**, *3* (11), 1726−1728.
(16) Dogutan, D. K.; McGuire, R.; Nocera, D. G. *J. Am. Chem. Soc.* **2011**, *133* (24), 9178−9180.
(17) McAlpin, J. G.; Stich, T. A.; Ohlin, C. A.; Surendranath, Y.; Nocera, D. G.; Casey, W. H.; Britt, R. D. *J. Am. Chem. Soc.* **2011**, *133* (39), 15444−15452.
(18) Meyer, T. J. *Nat. Chem.* **2011**, *3* (10), 757−758.
(19) Pijpers, J. J. H.; Winkler, M. T.; Surendranath, Y.; Buonassisi, T.; Nocera, D. G. *Proc. Natl. Acad. Sci. U. S. A.* **2011**, *108* (25), 10056−10061.
(20) Reece, S. Y.; Hamel, J. A.; Sung, K.; Jarvi, T. D.; Esswein, A. J.; Pijpers, J. J. H.; Nocera, D. G. *Science* **2011**, *334* (6056), 645−648.
(21) Schley, N. D.; Blakemore, J. D.; Subbaiyan, N. K.; Incarvito, C. D.; D'Souza, F.; Crabtree, R. H.; Brudvig, G. W. *J. Am. Chem. Soc.* **2011**, *133* (27), 10473−10481.
(22) Young, E. R.; Costi, R.; Paydavosi, S.; Nocera, D. G.; Bulovic, V. *Energy Environ. Sci.* **2011**, *4* (6), 2058−2061.
(23) Barber, J. *Cold Spring Harbor Symp. Quant. Biol.* **2012**, *77*, 295−307.
(24) Barnett, S. M.; Goldberg, K. I.; Mayer, J. M. *Nat. Chem.* **2012**, *4* (6), 498−502.
(25) Costi, R.; Young, E. R.; Bulović, V.; Nocera, D. G. *ACS Appl. Mater. Interfaces* **2013**, *5* (7), 2364−2367.
(26) Barnett, S. M.; Waidmann, C. R.; Scheuermann, M. L.; Nesvet, J. C.; Goldberg, K.; Mayer, J. M. In *Molecular Water Oxidation Catalysis*; John Wiley & Sons, Ltd: 2014; pp 187−210.
(27) Chadwick Ellis, W.; McDaniel, N. D.; Bernhard, S. In *Molecular Water Oxidation Catalysis*; John Wiley & Sons, Ltd: 2014; pp 153−162.
(28) Francàs, L.; Bofill, R.; García-Antón, J.; Escriche, L.; Sala, X.; Llobet, A. In *Molecular Water Oxidation Catalysis*; John Wiley & Sons, Ltd: 2014; pp 29−50.
(29) Woods, J. A.; Bernhard, S.; Albrecht, M. In *Molecular Water Oxidation Catalysis*; John Wiley & Sons, Ltd: 2014; pp 113−133.
(30) Fillol, J. L.; Codolà, Z.; Garcia-Bosch, I.; Gómez, L.; Pla, J. J.; Costas, M. *Nat. Chem.* **2011**, *3* (10), 807−813.
(31) Duan, L.; Bozoglian, F.; Mandal, S.; Stewart, B.; Privalov, T.; Llobet, A.; Sun, L. *Nat. Chem.* **2012**, *4* (5), 418−423.
(32) Rabten, W.; Kärkäs, M. D.; Åkermark, T.; Chen, H.; Liao, R.-Z.; Tinnis, F.; Sun, J.; Siegbahn, P. E. M.; Andersson, P. G.; Åkermark, B. *Inorg. Chem.* **2015**, *54* (10), 4611−4620.
(33) Mognon, L.; Mandal, S.; Castillo, C. E.; Fortage, J.; Molton, F.; Aromi, G.; Benet-Buchhlolz, J.; Collomb, M.-N.; Llobet, A. *Chem. Sci.* **2016**, *7* (5), 3304−3312.
(34) Moonshiram, D.; Jurss, J. W.; Concepcion, J. J.; Zakharova, T.; Alperovich, I.; Meyer, T. J.; Pushkar, Y. *J. Am. Chem. Soc.* **2012**, *134* (10), 4625−4636.
(35) Sundstrom, E. J.; Yang, X.; Thoi, V. S.; Karunadasa, H. I.; Chang, C. J.; Long, J. R.; Head-Gordon, M. *J. Am. Chem. Soc.* **2012**, *134* (11), 5233−5242.
(36) Bediako, D. K.; Surendranath, Y.; Nocera, D. G. *J. Am. Chem. Soc.* **2013**, *135* (9), 3662−3674.
(37) Hirahara, M.; Ertem, M. Z.; Komi, M.; Yamazaki, H.; Cramer, C. J.; Yagi, M. *Inorg. Chem.* **2013**, *52* (11), 6354−6364.
(38) *Molecular Water Oxidation Catalysts: A Key Topic for New Sustainable Energy Conversion Schemes*; Wiley: 2014.
(39) Ertem, M. Z.; Gagliardi, L.; Cramer, C. J. *Chem. Sci.* **2012**, *3* (4), 1293−1299.
(40) Fernando, A.; Aikens, C. M. *J. Phys. Chem. C* **2015**, *119* (20), 11072−11085.
(41) Garand, E.; Fournier, J. A.; Kamrath, M. Z.; Schley, N. D.; Crabtree, R. H.; Johnson, M. A. *Phys. Chem. Chem. Phys.* **2012**, *14* (29), 10109−10113.
(42) Marsh, B. M.; Zhou, J.; Garand, E. *J. Phys. Chem. A* **2014**, *118* (11), 2063−2071.
(43) Duffy, E. M.; Marsh, B. M.; Garand, E. *J. Phys. Chem. A* **2015**, *119* (24), 6326−6332.
(44) Marsh, B. M.; Voss, J. M.; Zhou, J.; Garand, E. *Phys. Chem. Chem. Phys.* **2015**, *17* (35), 23195−23206.
(45) Wolk, A. B.; Leavitt, C. M.; Fournier, J. A.; Kamrath, M. Z.; Wijeratne, G. B.; Jackson, T. A.; Johnson, M. A. *Int. J. Mass Spectrom.* **2013**, *354*−*355*, 33−38.
(46) Ingram, A. J.; Wolk, A. B.; Flender, C.; Zhang, J.; Johnson, C. J.; Hintermair, U.; Crabtree, R. H.; Johnson, M. A.; Zare, R. N. *Inorg. Chem.* **2014**, *53* (1), 423−433.
(47) Zhang, M.; de Respinis, M.; Frei, H. *Nat. Chem.* **2014**, *6* (4), 362−367.
(48) Duffy, E. M.; Marsh, B. M.; Voss, J. M.; Garand, E. *Angew. Chem., Int. Ed.* **2016**, *55* (12), 4079−4082.
(49) Gardenier, G. H.; Johnson, M. A.; McCoy, A. B. *J. Phys. Chem. A* **2009**, *113* (16), 4772−4779.
(50) Mizuse, K.; Kuo, J.-L.; Fujii, A. *Chem. Sci.* **2011**, *2* (5), 868−876.
(51) Mizuse, K.; Fujii, A. *J. Phys. Chem. A* **2013**, *117* (5), 929−938.
(52) Sodupe, M.; Bertran, J.; Rodríguez-Santiago, L.; Baerends, E. J. *J. Phys. Chem. A* **1998**, *103* (1), 166−170.
(53) Livshits, E.; Baer, R. *J. Phys. Chem. A* **2008**, *112* (50), 12789−12791.
(54) Pieniazek, P. A.; VandeVondele, J.; Jungwirth, P.; Krylov, A. I.; Bradforth, S. E. *J. Phys. Chem. A* **2008**, *112* (27), 6159−6170.
(55) Cheng, Q.; Evangelista, F. A.; Simmonett, A. C.; Yamaguchi, Y.; Schaefer, H. F. *J. Phys. Chem. A* **2009**, *113* (49), 13779−13789.
(56) Pieniazek, P. A.; Sundstrom, E. J.; Bradforth, S. E.; Krylov, A. I. *J. Phys. Chem. A* **2009**, *113* (16), 4423−4429.
(57) Kamarchik, E.; Kostko, O.; Bowman, J. M.; Ahmed, M.; Krylov, A. I. *J. Chem. Phys.* **2010**, *132* (19), 194311−11.
(58) Do, H.; Besley, N. A. *Phys. Chem. Chem. Phys.* **2013**, *15* (38), 16214−16219.
(59) Marsalek, O.; Elles, C. G.; Pieniazek, P. A.; Pluhařová, E.; VandeVondele, J.; Bradforth, S. E.; Jungwirth, P. *J. Chem. Phys.* **2011**, *135* (22), 224510.
(60) Svoboda, O.; OnCak, M.; SlaviCek, P. *J. Chem. Phys.* **2011**, *135* (15), 154301−16.
(61) Do, H.; Besley, N. A. *J. Phys. Chem. A* **2013**, *117* (25), 5385−5391.
(62) Lu, E.-P.; Pan, P.-R.; Li, Y.-C.; Tsai, M.-K.; Kuo, J.-L. *Phys. Chem. Chem. Phys.* **2014**, *16* (35), 18888−18895.
(63) Lv, Z.-L.; Xu, K.; Cheng, Y.; Chen, X.-R.; Cai, L.-C. *J. Chem. Phys.* **2014**, *141* (5), 054309.
(64) Herr, J. D.; Steele, R. P. *J. Phys. Chem. A* **2016**, DOI: 10.1021/acs.jpca.6b07465.
(65) Herr, J. D.; Talbot, J.; Steele, R. P. *J. Phys. Chem. A* **2015**, *119* (4), 752−766.
(66) Møller, C.; Plesset, M. S. *Phys. Rev.* **1934**, *46* (7), 618−622.
(67) Dunning, T. H. *J. Chem. Phys.* **1989**, *90* (2), 1007−1023.
(68) Kendall, R. A.; Dunning, T. H.; Harrison, R. J. *J. Chem. Phys.* **1992**, *96* (9), 6796−6806.
(69) Scott, A. P.; Radom, L. *J. Phys. Chem.* **1996**, *100* (41), 16502−16513.
(70) Rowe, D. J. *Rev. Mod. Phys.* **1968**, *40* (1), 153−166.
(71) Emrich, K. *Nucl. Phys. A* **1981**, *351* (3), 379−396.

DOI: 10.1021/jacs.6b07182
J. Am. Chem. Soc. 2016, 138, 11936−11945

(72) Stanton, J. F.; Bartlett, R. J. *J. Chem. Phys.* **1993**, *98* (9), 7029−7039.
(73) Krylov, A. I. *Annu. Rev. Phys. Chem.* **2008**, *59* (1), 433−462.
(74) Cizek, J. *J. Chem. Phys.* **1966**, *45* (11), 4256−4266.
(75) Bartlett, R. J.; Musiał, M. *Rev. Mod. Phys.* **2007**, *79* (1), 291−352.
(76) Feyereisen, M.; Fitzgerald, G.; Komornicki, A. *Chem. Phys. Lett.* **1993**, *208* (5−6), 359−363.
(77) Vahtras, O.; Almlöf, J.; Feyereisen, M. W. *Chem. Phys. Lett.* **1993**, *213* (5−6), 514−518.
(78) Eichkorn, K.; Treutler, O.; Öhm, H.; Häser, M.; Ahlrichs, R. *Chem. Phys. Lett.* **1995**, *240* (4), 283−290.
(79) Weigend, F.; Häser, M.; Patzelt, H.; Ahlrichs, R. *Chem. Phys. Lett.* **1998**, *294* (1−3), 143−152.
(80) Jung, Y.; Sodt, A.; Gill, P. M. W.; Head-Gordon, M. *Proc. Natl. Acad. Sci. U. S. A.* **2005**, *102* (19), 6692−6697.
(81) Distasio, R. A.; Steele, R. P.; Rhee, Y. M.; Shao, Y.; Head-Gordon, M. *J. Comput. Chem.* **2007**, *28* (5), 839−856.
(82) Shao, Y.; Gan, Z.; Epifanovsky, E.; Gilbert, A. T. B.; Wormit, M.; Kussmann, J.; Lange, A. W.; Behn, A.; Deng, J.; Feng, X.; Ghosh, D.; Goldey, M.; Horn, P. R.; Jacobson, L. D.; Kaliman, I.; Khaliullin, R. Z.; Kuś, T.; Landau, A.; Liu, J.; Proynov, E. I.; Rhee, Y. M.; Richard, R. M.; Rohrdanz, M. A.; Steele, R. P.; Sundstrom, E. J.; Woodcock, H. L.; Zimmerman, P. M.; Zuev, D.; Albrecht, B.; Alguire, E.; Austin, B.; Beran, G. J. O.; Bernard, Y. A.; Berquist, E.; Brandhorst, K.; Bravaya, K. B.; Brown, S. T.; Casanova, D.; Chang, C.-M.; Chen, Y.; Chien, S. H.; Closser, K. D.; Crittenden, D. L.; Diedenhofen, M.; DiStasio, R. A.; Do, H.; Dutoi, A. D.; Edgar, R. G.; Fatehi, S.; Fusti-Molnar, L.; Ghysels, A.; Golubeva-Zadorozhnaya, A.; Gomes, J.; Hanson-Heine, M. W. D.; Harbach, P. H. P.; Hauser, A. W.; Hohenstein, E. G.; Holden, Z. C.; Jagau, T.-C.; Ji, H.; Kaduk, B.; Khistyaev, K.; Kim, J.; Kim, J.; King, R. A.; Klunzinger, P.; Kosenkov, D.; Kowalczyk, T.; Krauter, C. M.; Lao, K. U.; Laurent, A. D.; Lawler, K. V.; Levchenko, S. V.; Lin, C. Y.; Liu, F.; Livshits, E.; Lochan, R. C.; Luenser, A.; Manohar, P.; Manzer, S. F.; Mao, S.-P.; Mardirossian, N.; Marenich, A. V.; Maurer, S. A.; Mayhall, N. J.; Neuscamman, E.; Oana, C. M.; Olivares-Amaya, R.; O'Neill, D. P.; Parkhill, J. A.; Perrine, T. M.; Peverati, R.; Prociuk, A.; Rehn, D. R.; Rosta, E.; Russ, N. J.; Sharada, S. M.; Sharma, S.; Small, D. W.; Sodt, A.; Stein, T.; Stück, D.; Su, Y.-C.; Thom, A. J. W.; Tsuchimochi, T.; Vanovschi, V.; Vogt, L.; Vydrov, O.; Wang, T.; Watson, M. A.; Wenzel, J.; White, A.; Williams, C. F.; Yang, J.; Yeganeh, S.; Yost, S. R.; You, Z.-Q.; Zhang, I. Y.; Zhang, X.; Zhao, Y.; Brooks, B. R.; Chan, G. K. L.; Chipman, D. M.; Cramer, C. J.; Goddard, W. A.; Gordon, M. S.; Hehre, W. J.; Klamt, A.; Schaefer, H. F.; Schmidt, M. W.; Sherrill, C. D.; Truhlar, D. G.; Warshel, A.; Xu, X.; Aspuru-Guzik, A.; Baer, R.; Bell, A. T.; Besley, N. A.; Chai, J.-D.; Dreuw, A.; Dunietz, B. D.; Furlani, T. R.; Gwaltney, S. R.; Hsu, C.-P.; Jung, Y.; Kong, J.; Lambrecht, D. S.; Liang, W.; Ochsenfeld, C.; Rassolov, V. A.; Slipchenko, L. V.; Subotnik, J. E.; Van Voorhis, T.; Herbert, J. M.; Krylov, A. I.; Gill, P. M. W.; Head-Gordon, M. *Mol. Phys.* **2015**, *113* (2), 184−215.
(83) Brites, V.; Lisy, J. M.; Gaigeot, M. P. *J. Phys. Chem. A* **2015**, *119* (11), 2468−2474.
(84) Cimas, A.; Vaden, T. D.; de Boer, T. S. J. A.; Snoek, L. C.; Gaigeot, M. P. *J. Chem. Theory Comput.* **2009**, *5* (4), 1068−1078.
(85) Thomas, M.; Brehm, M.; Fligg, R.; Vohringer, P.; Kirchner, B. *Phys. Chem. Chem. Phys.* **2013**, *15* (18), 6608−6622.
(86) Kucar, J.; Meyer, H. D.; Cederbaum, L. S. *Chem. Phys. Lett.* **1987**, *140* (5), 525−530.
(87) Meyer, H. D.; Manthe, U.; Cederbaum, L. S. *Chem. Phys. Lett.* **1990**, *165* (1), 73−78.
(88) Vendrell, O.; Brill, M.; Gatti, F.; Lauvergnat, D.; Meyer, H.-D. *J. Chem. Phys.* **2009**, *130* (23), 234305.
(89) Wang, H. *J. Phys. Chem. A* **2015**, *119* (29), 7951−7965.
(90) Sibert, E. L. *J. Chem. Phys.* **1988**, *88* (7), 4378−4390.
(91) Barone, V. *J. Chem. Phys.* **2005**, *122* (1), 014108.
(92) Bloino, J.; Biczysko, M.; Barone, V. *J. Phys. Chem. A* **2015**, *119* (49), 11862−11874.
(93) VÁZquez, J.; Stanton, J. F. *Mol. Phys.* **2006**, *104* (3), 377−388.
(94) Carter, S.; Culik, S. J.; Bowman, J. M. *J. Chem. Phys.* **1997**, *107* (24), 10458−10469.
(95) Carter, S.; Bowman, J. M.; Handy, N. C. *Theor. Chem. Acc.* **1998**, *100* (1−4), 191−198.
(96) Christiansen, O. *Phys. Chem. Chem. Phys.* **2012**, *14* (19), 6672−6687.
(97) Matsunaga, N.; Chaban, G. M.; Gerber, R. B. *J. Chem. Phys.* **2002**, *117* (8), 3541−3547.
(98) Cheng, X.; Steele, R. P. *J. Chem. Phys.* **2014**, *141* (10), 104105.
(99) Panek, P. T.; Jacob, C. R. *ChemPhysChem* **2014**, *15* (15), 3365−3377.
(100) Christiansen, O. *J. Chem. Phys.* **2004**, *120* (5), 2149−2159.
(101) Thompson, T. C.; Truhlar, D. G. *Chem. Phys. Lett.* **1980**, *75* (1), 87−90.
(102) Neff, M.; Rauhut, G. *J. Chem. Phys.* **2009**, *131* (12), 124129.
(103) Hanson-Heine, M. W. D. *J. Chem. Phys.* **2016**, *144* (20), 204116.
(104) Zimmerman, P. M.; Smereka, P. *J. Chem. Theory Comput.* **2016**, *12* (4), 1883−1891.
(105) Molina, A.; Smereka, P.; Zimmerman, P. M. *J. Chem. Phys.* **2016**, *144* (12), 124111.
(106) Roy, T. K.; Gerber, R. B. *Phys. Chem. Chem. Phys.* **2013**, *15* (24), 9468−9492.
(107) McCoy, A. B.; Guasco, T. L.; Leavitt, C. M.; Olesen, S. G.; Johnson, M. A. *Phys. Chem. Chem. Phys.* **2012**, *14* (20), 7205−7214.
(108) Stathopoulos, A.; McCombs, J. R. *ACM Trans. Math. Softw.* **2010**, *37* (2), 1−30.
(109) Philip, R. B.; Per, J. *Molecular Symmetry and Spectroscopy*, 2nd ed.; NRC Research Press: 2006; p 748.
(110) Herzberg, G. *Molecular Spectra and Molecular Structure*, 2nd ed.; D. Van Nostrand Company, Inc.: Princeton, NJ, 1950; Vol. *1*.
(111) *Origin*; OriginLab: Northampton, MA, 2016.
(112) Szabo, A.; Ostlund, N. S. *Modern Quantum Chemistry*; McGraw-Hill, Inc.: New York, 1989.
(113) Barone, V.; Biczysko, M.; Bloino, J.; Cimino, P.; Penocchio, E.; Puzzarini, C. *J. Chem. Theory Comput.* **2015**, *11* (9), 4342−4363.
(114) Biczysko, M.; Latajka, Z. *J. Phys. Chem. A* **2002**, *106* (13), 3197−3201.
(115) Pereverzev, A. Y.; Cheng, X.; Nagornova, N. S.; Reese, D. L.; Steele, R. P.; Boyarkin, O. V. *J. Phys. Chem. A* **2016**, *120* (28), 5598−5608.
(116) Relph, R. A.; Guasco, T. L.; Elliott, B. M.; Kamrath, M. Z.; McCoy, A. B.; Steele, R. P.; Schofield, D. P.; Jordan, K. D.; Viggiano, A. A.; Ferguson, E. E.; Johnson, M. A. *Science* **2010**, *327* (5963), 308−312.
(117) Johnson, C. J.; Wolk, A. B.; Fournier, J. A.; Sullivan, E. N.; Weddle, G. H.; Johnson, M. A. *J. Chem. Phys.* **2014**, *140* (22), 221101.
(118) Kamrath, M. Z.; Garand, E.; Jordan, P. A.; Leavitt, C. M.; Wolk, A. B.; Van Stipdonk, M. J.; Miller, S. J.; Johnson, M. A. *J. Am. Chem. Soc.* **2011**, *133* (16), 6440−6448.
(119) Guasco, T. L.; Johnson, M. A.; McCoy, A. B. *J. Phys. Chem. A* **2011**, *115* (23), 5847−5858.
(120) Bandyopadhyay, B.; Reishus, K. N.; Duncan, M. A. *J. Phys. Chem. A* **2013**, *117* (33), 7794−7803.
(121) Cheng, T. C.; Bandyopadhyay, B.; Mosley, J. D.; Duncan, M. A. *J. Am. Chem. Soc.* **2012**, *134* (31), 13046−13055.
(122) Burke, N. L.; DeBlase, A. F.; Redwine, J. G.; Hopkins, J. R.; McLuckey, S. A.; Zwier, T. S. *J. Am. Chem. Soc.* **2016**, *138* (8), 2849−2857.

DOI: 10.1021/jacs.6b07182
J. Am. Chem. Soc. 2016, 138, 11936−11945